nature water

Article

https://doi.org/10.1038/s44221-023-00095-4

Electrodialytic crystallization to enable zero liquid discharge

Received: 17 December 2022

Accepted: 12 May 2023

Published online: 12 June 2023

Check for updates

Xudong Zhang[1,4], Yiqun Yao[2,4], Thomas Horseman[3,4], Ruoyu Wang[1], Yiming Yin[2], Sizhuo Zhang[1], Tiezheng Tong[2] & Shihong Lin[1,3]

The management of hypersaline brines (that is, wastewater of high salinity) is a technical challenge that has received increasing attention due to their growing volume, environmental impacts and increasingly stringent regulations. Here we present electrodialytic crystallization (EDC) as a new process to achieve brine crystallization without evaporation. In an EDC process, the brine stream recirculating between an electrodialysis cell and a crystallizer remains oversaturated via continuous electromigration of ions from the feed stream across the ion exchange membranes. We first used Na_2SO_4 as the model salt to demonstrate the feasibility of EDC and to perform a systematic investigation of how crystallization kinetics and crystal size distribution depend on current density and crystallization mode. We then elucidated the criterion of crystallizability and showed how it depends on salt species, membrane properties and operating conditions. Lastly, we analysed the energy consumption of an EDC-reverse osmosis treatment train for achieving zero liquid discharge of a Na_2SO_4 brine. Overall, this study provides a proof of concept for EDC as an electric-field driven and non-evaporative crystallization process, and lays the foundation for its future technical development and optimization.

The management of hazardous high-salinity brines represents a prominent environmental challenge to water sustainability[1,2]. A large volume of highly saline brines is generated from the energy, mining and desalination industries[1,3–7]. The current brine management commonly relies on evaporation ponds or injection into deep subterranean formations, which are plagued with the concerns of induced seismicity, negative impacts on groundwater, and the removal of accessible water from the hydrologic cycle[1,8–10]. Therefore, zero liquid discharge (ZLD) is the preferred brine management approach and a key component of water circularity[11]. However, achieving cost-effective ZLD is technically challenging due to the very high salinity (that is, total dissolved solid, or TDS) of the brines. The state-of-the-art desalination process, reverse osmosis (RO), can only concentrate the brines to a limited level of TDS (dependent on the specific composition of the brine)[1,10]. Consequently, current ZLD systems dominantly rely on evaporative methods to concentrate high-salinity brines and attain crystallization.

Evaporative processes are intrinsically energy intensive due to liquid-to-vapour phase change. The latent heat of vapourization (>650 kWh m^{-3}) is nearly two orders of magnitude higher than the Gibbs free energy of ZLD (typically <10 kWh m^{-3}) (refs. 2,12). Mechanical vapour compression (MVC) is currently the most mature technology for ZLD due to its excellent performance in latent heat recovery[1]. Nonetheless, MVC is still energy intensive, typically consuming 30–40 kWh_e m^{-3} (subscript 'e' for electricity) for brine concentration (up to 160–300 g l^{-1} TDS) and >50 kWh_e m^{-3} for crystallization[13–15]. Further, MVC requires high capital cost due to the use of expensive materials to prevent corrosion caused by the boiling brine[1]. In one example of using MVC for ZLD[16], the brine concentration and crystallization steps contributed to ~90% of the total ZLD cost (including the preceding pre-treatment

[1]Department of Civil and Environmental Engineering, Vanderbilt University, Nashville, TN, USA. [2]Department of Civil and Environmental Engineering, Colorado State University, Fort Collins, CO, USA. [3]Department of Chemical and Biomolecular Engineering, Vanderbilt University, Nashville, TN, USA. [4]These authors contributed equally: Xudong Zhang, Yiqun Yao, Thomas Horseman. e-mail: tiezheng.tong@colostate.edu; shihong.lin@vanderbilt.edu

https://doi.org/10.1038/s44221-023-00095-4

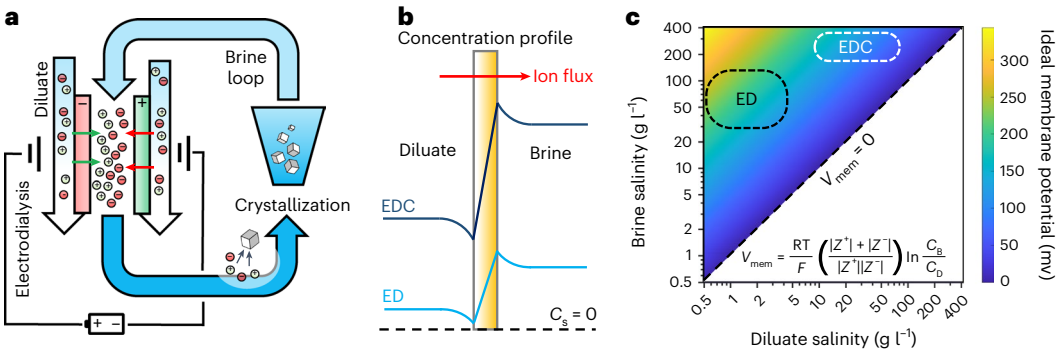

Fig. 1 | The concept of EDC. a, Schematic illustration of the EDC: ions in the diluate streams are pulled to the recirculated brine loop where the salt concentration exceeds the saturation limit, resulting in precipitation of salt crystals. **b**, Representative concentration profiles of counter ions across an IEM (either CEM or AEM) for EDC versus ED. The profiles are only depicted for comparing the relative levels of concentrations (not to scale). **c**, Membrane potential as a function of brine and diluate salinities following the equation shown in the figure. The plot is generated using NaCl (as an example) and applying the approximation of ideal solution throughout the range of salinity. The derivation of the membrane potential is presented in Supplementary Section 1. While the value of V_{mem} may change with more accurate evaluation (for example, using activities) and with other salts, the comparison of V_{mem} between ED and EDC should be generally valid.

and RO steps), with the crystallization step processing only 12% of the overall wastewater volume but accounting for 41% of the treatment cost. Developing non-evaporative processes that enable brine crystallization, therefore, will have a transformative impact by substantially reducing the cost, energy consumption and carbon footprint of ZLD.

Electrodialysis (ED) is an electrochemical separation process that has been used in various desalination applications[17,18] and explored for concentrating RO brine before it is sent to MVC-based brine concentrator and crystallizer[19–21]. In a conventional ED process, saline feed water enters an ED stack comprising multiple pairs of cation exchange membranes (CEMs) and anion exchange membranes (AEMs) placed alternately. Under an applied electric field, ions in the feed channels migrate to the two adjacent brine channels, producing a diluate stream with a reduced salinity and brine streams with a higher salinity. Despite its ability to achieve higher brine salinities than conventional RO (due to the limited operating pressure of existing RO systems), current ED systems can at best function as a brine concentrating unit for volume reduction but cannot achieve crystallization[1,22].

In this Article, we introduce a novel variant of ED that electrifies brine crystallization without a subsequent MVC or any evaporative process. This new process, namely electrodialytic crystallization (EDC), integrates ED with a crystallizer in a way that the brine stream is constantly recirculated between the brine channels of the ED cell and the crystallizer. Under an applied electric field, ions in the feed stream are constantly drawn to the recirculated brine stream, which pushes the brine stream concentration beyond the salt's solubility limit and thereby induces salt crystallization (Fig. 1a). This process, to the best of our knowledge, represents the first technology that achieves electric field-driven brine crystallization.

EDC differs from conventional ED in several aspects. While there are two effluent streams (that is, diluate and brine streams) in an ED process, there is only one effluent stream (that is, diluate stream) for an EDC system. Compared with conventional ED, EDC is designed to work with a higher feed concentration to achieve a higher brine concentration (Fig. 1b). Despite a larger trans-membrane concentration difference to overcome, the minimum energy to transfer an ion in EDC can be lower than ED because the membrane potential (or Donnan potential) is dependent on the ratio, but not the difference, of ion concentrations across the membrane (Fig. 1c). The membrane potential of the EDC can be relatively low as salinities in both the feed and brine channels are at the same order of magnitude.

In this study, we first prove the concept of EDC using high-concentration Na_2SO_4 brines. We evaluate the impacts of current density and operation mode on crystallization kinetics and the morphology of the produced salt crystals. We then investigate the performance of EDC using multiple salt species and establish a theoretical framework to determine salt crystallizability (that is, the ability of a salt to be crystallized) in EDC, elucidating the dependence of crystallizability on salt species and operating conditions. Lastly, we estimate the energy consumption of an integrated EDC-RO system for ZLD (EDC is integrated with RO as EDC alone is either incapable of, or inefficient for, achieving ZLD).

Proof of concept with Na_2SO_4: kinetics and crystal size

The feasibility of EDC was demonstrated using a bench-scale system with a recirculated stream of Na_2SO_4 solution (initially at 63.5 g l^{-1}) as the diluate. The brine loop contained a solution of 174 g l^{-1} Na_2SO_4 (that is, its solubility at 20 °C). The supernatant of the crystallizer was filtered using crossflow microfiltration (MF) before re-entering the ED cell to minimize clogging the brine channel of the ED cell by crystals (Fig. 2a). Two operating modes, namely continuous and batch modes, were used to evaluate EDC performance (Fig. 2b). In the continuous mode, the temperature of the crystallizer was controlled at 18 °C and salt crystals were continuously generated in the crystallizer. In the batch mode, no temperature control was applied to the crystallizer, but brine collected from the crystallizer was cooled to 18 °C in an external water bath for an extended period of time to maximize crystal production. While the continuous mode is more practically relevant, the batch mode provides an upper limit of crystal production by removing the constraint of crystallization kinetics.

We evaluated the impact of current density on the crystallization kinetics using three current densities (that is, 20, 40 and 60 mA cm^{-2}). EDC was able to produce Na_2SO_4 crystals at all the tested current densities, as the total suspended solids (TSS, that is, mass of crystal particles per volume of water) increased over time (Fig. 2c). The reported TSS have been corrected for background precipitation from the solubility difference between 20 °C (the temperature at which the initial brine was prepared) and 18 °C (the temperature in the crystallizer), and thus reflect crystal production only due to trans-membrane ion transport (Methods and Supplementary Section 2).

Regardless of current density, the TSS obtained with the batch mode was higher than that with the continuous mode at the beginning stage of the experiments, which was probably due to the limited crystallization kinetics. In the batch mode, the TSS was roughly linear to operation time and the slope was approximately proportional to current density (Supplementary Fig. 2 and Supplementary Table 6).

https://doi.org/10.1038/s44221-023-00095-4

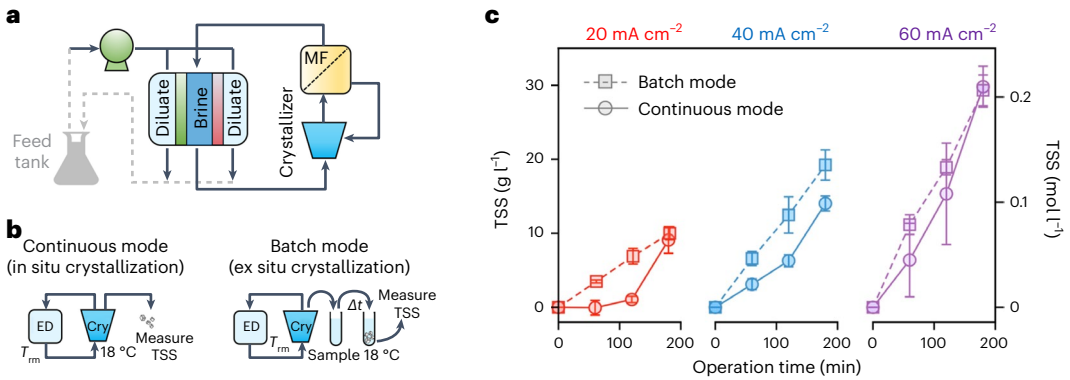

Fig. 2 | Proof of concept for EDC with experiments of Na_2SO_4 crystallization. **a**, Schematic of the experimental setup for EDC experiments, integrating an ED cell, a crystallizer and an MF unit. The recirculation of the feed stream (grey components) was applied in our bench-scale experiments. **b**, Comparison between continuous mode, where crystallization occurs within the EDC system, and batch mode, where crystallization occurs external to the EDC system. **c**, TSS in both g l^{-1} (left) and mol l^{-1} (right) as a function of operation time with different operating modes and current densities (20, 40 and 60 mA cm^{-2}). In the continuous mode, the brine temperature in the crystallizer was maintained at 18 °C and crystals were in situ produced and measured, while in the batch mode, the EDC system was operated at room temperature and crystals were produced in an 18 °C water bath and then measured. The ED cell comprises two pairs of the standard IEMs. The initial diluate was 2 litres of 6 wt% (63.5 g l^{-1}) Na_2SO_4, while the initial brine was 1 litre of saturated Na_2SO_4 (174 g l^{-1}, corresponding to Na_2SO_4 solubility at 20 °C). The error bars in **c** represent standard deviation from at least three replicates and may stem from uncertainty in TSS sampling (due to the spatial heterogeneity in particle dispersion) and the stochasticity of precipitation process[31]. These factors may have led to high uncertainty at a higher current density that generates more and larger crystals.

In continuous mode, however, crystals may not form when the brine concentration reached or even exceeded Na_2SO_4 solubility, which led to oversaturation of the brine. As the TSS values from the batch mode were measured after sufficient precipitation time (that is, the TSS was measured after the TDS stopped decreasing), they more closely represent what could theoretically be extracted when the brines reach equilibrium. Given more time for crystallization, continuous mode EDC could generate as much TSS as batch mode EDC towards the end of the 3 h experiments (Fig. 2c).

The particle size distributions of the Na_2SO_4 crystals produced by EDC using continuous mode depend on both current density and operation time (Fig. 3). In general, the Na_2SO_4 crystals have an average particle size (diameter) of hundreds of micrometres (Fig. 3a–d). The average particle size at the same crystallization time increased systematically with a higher current density. At 20 mA cm^{-2}, no substantial change of particle size was observed with a longer crystallization time (Fig. 3a,d). In comparison, the particles grew larger with a wider size distribution over a longer crystallization time when the current densities were 40 and 60 mA cm^{-2} (Fig. 3b–d). Regardless of current density, batch mode EDC generated much larger, centimetre-scale, crystals (Fig. 3e).

Considering that sparingly soluble salts are prone to form during hypersaline brine treatment, we evaluated the potential effects of gypsum ($CaSO_4{\bullet}2H_2O$) scaling (a common type of scaling in membrane desalination[23,24]) on the EDC performance in Na_2SO_4 crystallization. The presence of supersaturated gypsum did not have a substantial impact on EDC performance, that is, the temporal evolutions of diluate and brine conductivity, voltage and TSS during 3 h were similar with and without gypsum (Supplementary Fig. 3), which suggests that EDC was not susceptible to gypsum scaling in our proof-of-concept experiments. Future work is needed for more comprehensive understanding of the mineral scaling in EDC (for example, effects of scalant types and operation durations).

Crystallizability criterion

In addition to Na_2SO_4, EDC was also tested for other highly soluble salts such as K_2SO_4, KNO_3, KCl and NaCl. In all experiments regardless of the salt type, we used 0.6 M of each salt as the feed solution and the saturated solution (at 20 °C) of the corresponding salt as the receiving brine. With the same ion exchange membranes (IEMs) we used for crystallizing Na_2SO_4, two additional salts, including K_2SO_4 and KNO_3, could be successfully crystallized by EDC (Fig. 4a). In all cases, the TSS obtained using batch mode at the same operation time was higher than that obtained using the continuous mode, which was probably caused by the limited crystallization kinetics as discussed in the previous section.

For KNO_3, the TSS extracted using EDC at 60 min was less than the background TSS obtained using the same conditions but without applied electrical potential (Supplementary Tables 2 and 4). Because the electric current generates heat within the ED cell and thus raises the temperature of the flow channels, small nucleates that may have formed in the crystallizer could redissolve in the brine channels of the ED cell (as the solubility of KNO_3 positively correlates with temperature, Supplementary Fig. 1) and thus slowed down the crystallization rate as compared with that when no current was applied. With longer operation (120 and 180 min), the growing degree of oversaturation due to continuous increase of brine concentration eventually outcompeted the effect of redissolution of small nucleates in the brine channel and led to the net formation of TSS (after subtracting background) in the crystallizer. The hypothesis of nucleate redissolution in a warm ED cell was further supported by EDC experiments without the MF cell, where the measured TSS of Na_2SO_4 was lower than the background TSS even after 3 h of experiment (Supplementary Fig. 4). The possible nucleate redissolution in a warm ED cell emphasizes the importance of integrating MF in the system to minimize formed crystals from entering the ED cell.

Using the same IEMs and operating conditions, the EDC process was unable to produce crystals using feed solutions of KCl and NaCl. This was because the brine concentrations of these salts did not exceed their solubilities to a sufficient extent, which is evident when we plot the total brine concentration as a function of operation time for the five tested salts and compare them with their respective solubilities (Fig. 4b). The total brine concentration is defined as the sum of TDS and TSS of the brine (in molarity) (Supplementary Section 6). For non-crystallizable salts, the total brine concentration is the TDS; for crystallizable salts, the total brine concentration can be interpreted as the imaginary TDS as if crystals never formed. For Na_2SO_4, K_2SO_4 and KNO_3 (crystallizable in Fig. 4b), the total brine concentrations increased consistently during the 3 h EDC operation and exceeded the solubility of the respective salts. For NaCl and KCl (non-crystallizable in Fig. 4b), however, the total brine concentration consistently decreased

https://doi.org/10.1038/s44221-023-00095-4

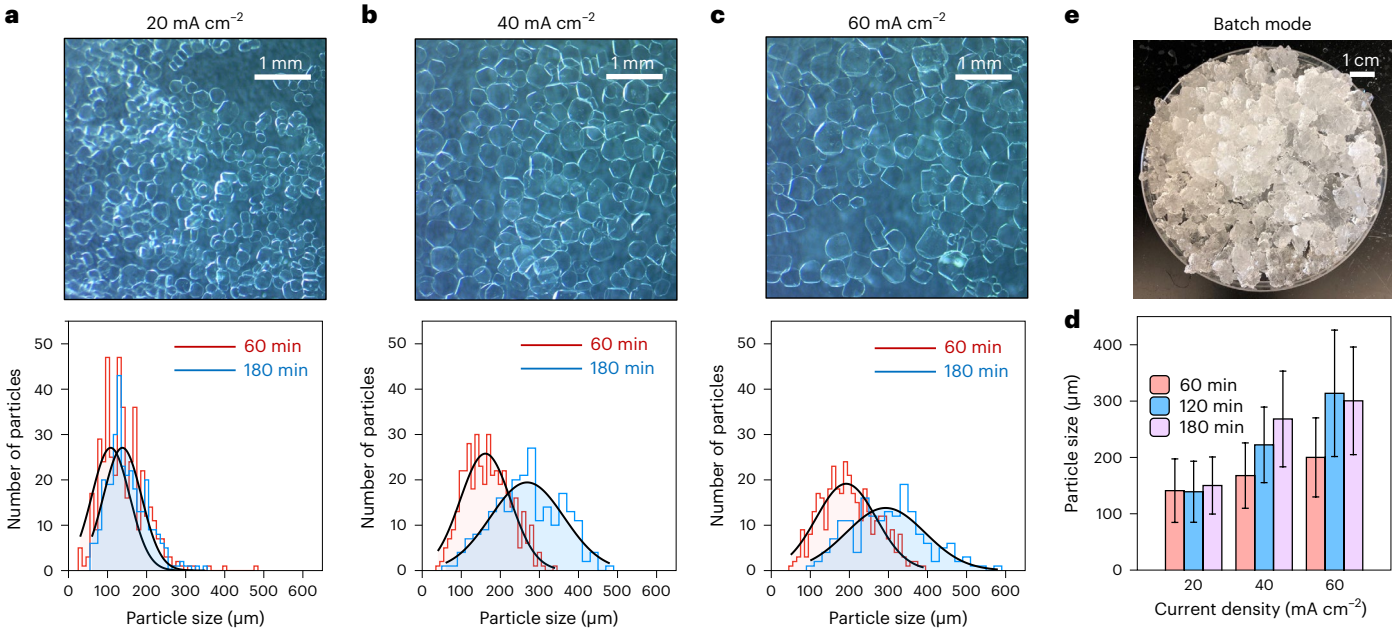

Fig. 3 | The variation of crystal size produced by EDC under different current densities. a–c, Optical crystal images after 180 min operation (top) and particle size distributions of crystals at 60 and 180 min (bottom) for continuous mode with current densities of 20 mA cm^{-2} (**a**), 40 mA cm^{-2} (**b**) and 60 mA cm^{-2} (**c**). **d**, Summary of average particle sizes and standard deviations (represented by the error bars) at different operation times and current densities. The statistical summary is based on data shown in **a–c**. **e**, An example of crystals collected from batch mode at a current density of 40 mA cm^{-2}.

and never exceeded the respective solubilities (under these specific experimental conditions).

Elucidating the dependence of crystallizability on salt species requires understanding the water and ion transport through IEM in an ED process. There are four major transport phenomena occurring simultaneously in ED (Fig. 4c): electromigration and diffusion of ions, and electro-osmosis and osmosis of water. The only intended phenomenon is the electromigration of ions, that is, the movement of ions under the applied electric field, while all other phenomena are 'parasitic' and detrimental to the objective of EDC to achieving salt crystallization. Diffusion of ions from the brine to feed solution occurs due to the presence of concentration gradient (higher salt concentration in the brine). As diffusion rate is proportional to the trans-membrane concentration difference according to Fick's law, (back)diffusion can be substantial in EDC with a large trans-membrane concentration difference.

Though unintended, water transport also occurs via both osmosis and electro-osmosis. Osmosis results from osmotic pressure difference due to the trans-membrane salt concentration difference. Specifically, the chemical potential of water is lower in the brine with a higher salt concentration than in the feed solution with a lower salt concentration. In addition to osmosis, the ions migrating across IEMs also 'drag' part of the water molecules in their hydration shells, which is referred to as electro-osmosis[21,25,26]. Both osmosis and electro-osmosis move water from the feed solution to the brine. Water transport is detrimental to salt crystallization in EDC because it increases the brine volume and tends to dilute the brine, which acts against ion electromigration towards enriching the brine beyond the salt solubility.

The analysis of both ion and water transport through the IEMs suggests that the necessary (but not sufficient) condition for crystallization is that the ratio of molar flux between salt and water in an EDC process, (J_s/J_w, where J_s and J_w are the molar fluxes of the salt and water, respectively) exceeds salt solubility expressed in molar ratio. When J_s/J_w is lower than salt solubility, the brine can never become saturated. Comparing J_s/J_w and the solubility for the six salts tested clearly show that the crystallizable salts (Na_2SO_4, K_2SO_4 and KNO_3 in blue) satisfied the necessary condition whereas the non-crystallizable ones (NaCl and KCl in red) did not (Fig. 4d).

While the solubility at a given temperature is an intrinsic property of the salt, J_s/J_w depends on salt properties, membrane properties and operating conditions. It is likely that hydration plays an important role in electro-osmosis. Salts comprising ions that are more strongly hydrated (Supplementary Section 7) will probably result in a great extent of electro-osmosis and thus a lower J_s/J_w with the same IEMs and operating conditions. When the membrane is made of a relatively hydrophobic material, dehydration may occur to shed off some water molecules in the hydrated shell and thereby reduce water transport[27,28]. Moreover, increasing current density has also been shown as effective in increasing J_s/J_w (ref. 29).

Following the above principles, we performed additional EDC experiments using NaCl and KCl but with different IEMs (Supplementary Table 8) and operating conditions (Supplementary Table 9). This alternative set of IEMs have substantially lower water uptakes than the reference IEMs used to collect results for Fig. 4a (Supplementary Fig. 5), which is beneficial to reducing water transport via osmosis and electro-osmosis[30]. The use of the low-water-uptake IEMs indeed boosted the J_s/J_w (Fig. 4d), but this measure alone was still inadequate for achieving KCl and NaCl crystallization. Using the low-water-uptake IEMs with additional measures including (1) applying a higher current density, (2) using a higher initial diluate concentration and (3) reducing the volume of the brine loop (for specific conditions, see Methods and Supplementary Table 9), we eventually pushed the brine concentration of KCl and NaCl beyond their respective solubilities (Fig. 4e) and observed the formation of salt crystals (Fig. 4f). Higher current density and initial diluate concentration both contributed to a higher J_s/J_w ratio, whereas a smaller brine volume allowed a faster increase in brine concentration for a given membrane area (which in turn promoted the formation of crystals within the experimental timeframe).

In the case of NaCl, only a small TSS was measured towards the end of the 3 h EDC experiments (Fig. 4f), despite the high current density (80 mA cm^{-2}) and feed concentration (4 mol l^{-1}). The formation of NaCl crystals seems to require a substantial degree of oversaturation

https://doi.org/10.1038/s44221-023-00095-4

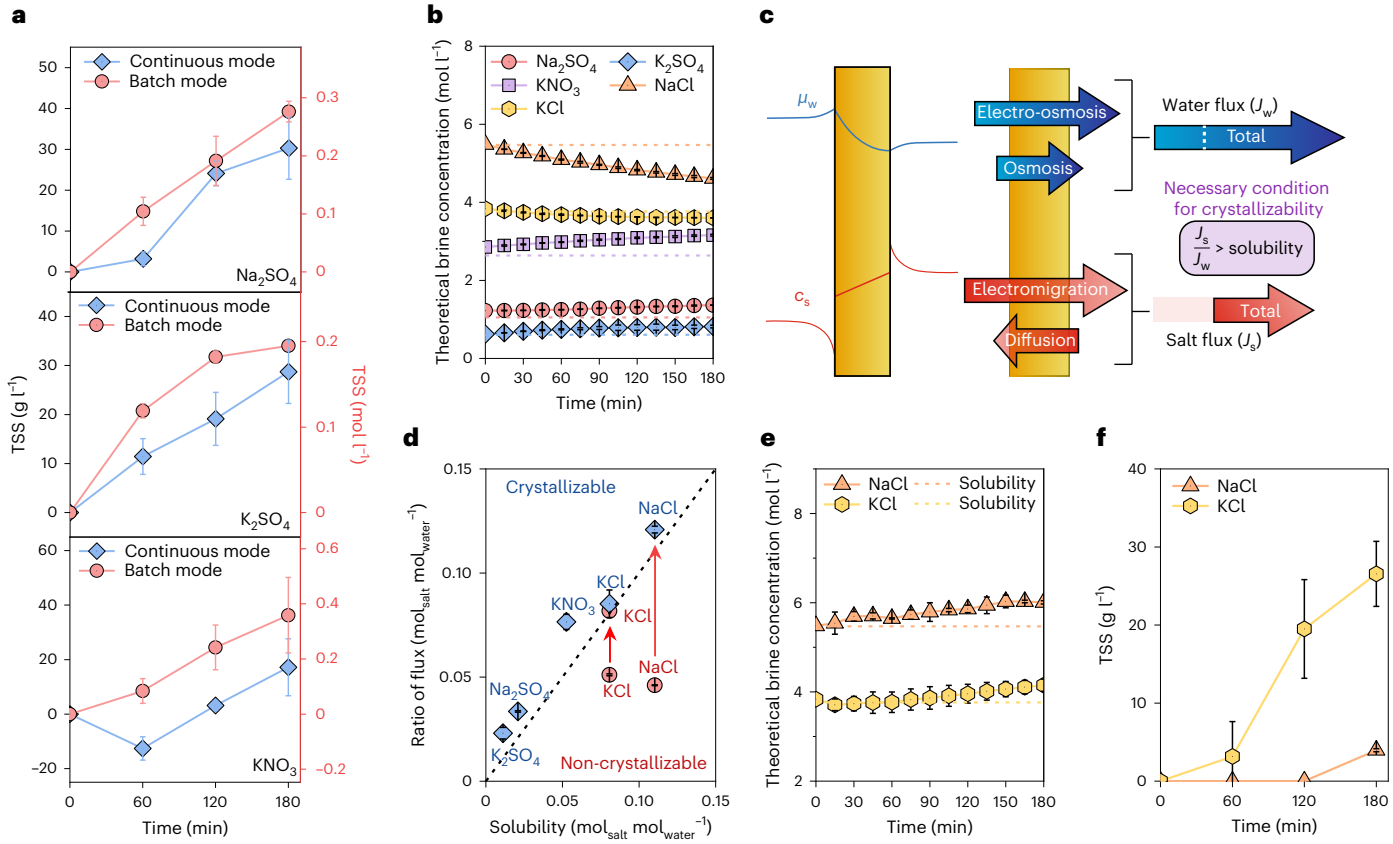

Fig. 4 | Crystallization of different salts in EDC. a, TSS production rates of Na_2SO_4, K_2SO_4 and KNO_3 with continuous and batch modes. The ED cell configured with five pairs of the IEMs. The applied current density was 40 mA cm^{-2}. The initial diluate was 4 litres of 0.6 M of each salt. The initial brine was 1 litre of saturated solution of the respective salt (at 20 °C). **b**, Theoretical brine concentration, that is, TDS plus TSS (if any), for five different salts. The operating conditions were the same as those for **a**. **c**, Schematic illustration of salt crystallization mechanism in the EDC system. **d**, Molar ratio of salt to water as calculated from the salt solubility at 18 °C (*x* axis) as compared with the ratio of salt flux to water flux in continuous mode (*y* axis). Blue rhombuses represent successful crystallization whereas red circles represent unsuccessful crystallization. **e**,**f**, Theoretical brine concentration (**e**) and TSS (**f**) for NaCl and KCl as a function of operation time with low-water-uptake IEMs and different operating conditions (details for operating conditions in each case can be found in Methods and Supplementary Section 5). The data and error bars in this figure represent the mean values and standard deviations of results from at least three replicates, respectively.

(Fig. 4e) and achieving a J_s/J_w ratio that exceeds solubility did not necessarily lead to crystallization (Fig. 4d). Therefore, the criterion of having a higher J_s/J_w than solubility is only a necessary, but not sufficient, condition for crystal formation. To achieve more efficient crystallization of NaCl, future research is needed to develop better membranes to minimize water transport with other strategies, such as coating IEMs with a surface layer that promotes ion dehydration[27].

Energy consumption of EDC and its integrated ZLD system

The energy consumptions of both EDC and the integrated ZLD treatment train comprising EDC and RO are estimated on the basis of experimental data (Supplementary Sections 8 and 9). The current analysis focuses on Na_2SO_4 for which data at different current densities were collected, noting that the results of the analysis can vary substantially depending on salt species, membrane properties and operating conditions. The crystal-specific energy consumption, that is, the energy (kWh) consumed to produce a unit mass (kg) of Na_2SO_4 crystals, strongly depends on current density (Fig. 5a), as a higher current density leads to a larger resistive loss. In addition to current density, the crystal-specific energy consumption also depends on crystal yield that quantifies the utilization efficiency of electrical current for crystal production. The crystal yield (η), defined as the measured TSS over theoretical maximum TSS calculated using the amount of charge transferred, varies between 40% and 60%. The crystal yield was not unity because (1) not all charge transfer resulted in ion transfer, that is, current efficiency was lower than unity; and (2) not all salt entering the brine loop can crystallize out due to the parasitic water transport and extra salt required to reach the sufficient level of oversaturation for crystallization. Clearly, η depends on salt species, membrane properties and operating conditions as these factors affect salt and water transport.

Using an EDC process alone to achieve ZLD (that is, converting the saline feed stream all the way to fresh water) is both highly inefficient or even infeasible. Instead, an EDC process should be coupled with an RO process to develop a treatment train for ZLD (Fig. 5b). In this integrated EDC-RO treatment train, the EDC effluent with a reduced (but still high) salinity is sent to the RO process for producing fresh water, and the RO brine mixes with the feed stream to re-enter the EDC unit. The specific energy consumption (SEC), that is, the energy (kWh) consumed to achieve ZLD for a unit volume (m^3) of feed water, was estimated for such an integrated EDC-RO ZLD system using a numerical model (Supplementary Section 9).

According to our analysis, the steady-state operation of EDC-RO demands that the salt rejection in ED (SR_{ED}), that is, the percentage reduction of the TDS of the ED feed stream as it flows through the ED cell, equals exactly the water recovery in the subsequent RO process (WR_{RO}). With increasing SR_{ED}, the SEC for the EDC unit increases whereas the SEC for the RO unit decreases (Fig. 5c). When

https://doi.org/10.1038/s44221-023-00095-4

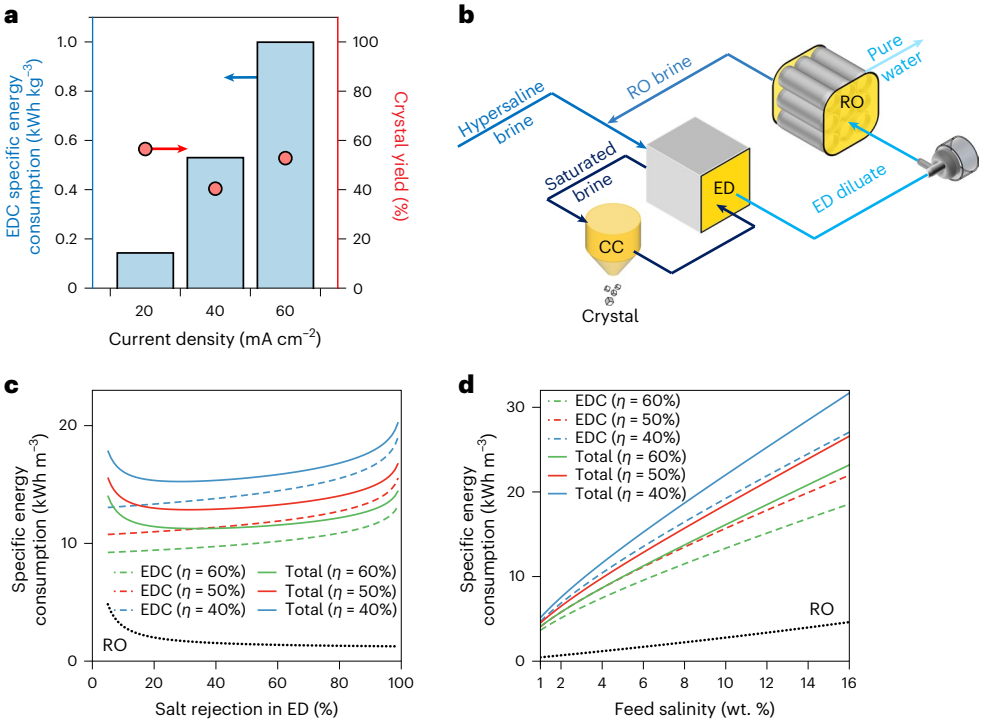

Fig. 5 | Energy consumption analysis of EDC and EDC-RO system for ZLD. **a**, The energy consumption and total efficiency of salt electromigration–crystallization in EDC system. Data were collected from Na_2SO_4 crystallization experiments of Fig. 2 in continuous mode. **b**, Schematic diagram of the integrated EDC-RO system. The salt rejection of the RO unit is assumed to be perfect and salt crystals are produced in crystal collector (CC). **c**, The energy consumption of EDC, RO and the integration process with varied salt rejections in the ED unit. The crystal yield efficiency is assumed to be 40%, 50% and 60%, respectively; the feed solution of the system is 6 wt% Na_2SO_4, and the applied current density is 20 mA cm^{-2}. **d**, The energy consumption of EDC, RO and the integration process with varied feed solution salinities. The crystal yield efficiency is assumed to be 40%, 50% and 60%, respectively; the salt rejection in the ED unit is 30%, and the applied current density is 20 mA cm^{-2}.

combined, the SEC of the overall EDC-RO process, SEC_{tot}, is a non-monotonic function of SR_{ED}. With very low SR_{ED} (<20%), SEC_{tot} is higher because the correspondingly low WR_{RO} demands that the diluate stream must recirculate more between the EDC and the RO units before it is recovered as RO permeate and the more recirculation results in more parasitic energy loss due to inefficient pressure recovery device. Throughout the most part of the analyzed range of SR_{ED} (10% to 80%), however, SEC_{tot} is largely insensitive to SR_{ED}. Obviously, the crystal yield, η, strongly affects SEC_{EDC}, which in turn influences SEC_{tot}.

We further extend our analysis to investigate the impact of feed stream salinity (Supplementary Section 9). Our analysis shows that SEC_{tot} monotonically increases with increasing feed salinity (Fig. 5d and Supplementary Fig. 12), which is not surprising as more salt needs to be removed from an EDC-RO system with a higher feed salinity. With a feed salinity of 12 wt% (the solubility of Na_2SO_4 at 20 °C is ~16 wt%), the SEC_{tot} at 20 mA cm^{-2} ranges from ~19 to ~26 kWh m^{-3}, depending on the crystal yield, and is lower than that of MVC-based brine concentrator and crystallizer. At higher current densities (for example, 40 and 60 mA cm^{-2}), the SEC_{tot} increases and becomes comparable to that of MVC (Supplementary Fig. 12). Although energy consumption is not the only consideration in technology comparison and MVC is versatile in crystallizing a wide variety of salts, EDC still represents a mechanistically new approach with the future potential to become a competitive crystallization process.

Conclusion and perspective

We have demonstrated in this study that EDC can crystallize several types of highly soluble salts from hypersaline solution (of single salt) using electric field without evaporation. The success of EDC for crystallization relies on the ability of promoting ion transport across IEMs without incurring excessive water transport, so that the brine concentration can exceed the solubility of the salt to be crystallized. Our analysis of the energy consumption for crystallizing Na_2SO_4 salt crystallization using an integrated EDC-RO system suggests that the EDC may have potential to become a competitive crystallization process for ZLD. Whether EDC and its integrated processes can become competitive for ZLD requires more in-depth and systematic analysis of how the crystallizability and the levelized cost of water depend on the salt type, operating conditions and membrane properties. Pilot-scale experiments are necessary in the future to understand the performance robustness and generate reliable data for techno-economic analysis. In addition, further improvement of EDC's energy efficiency and its applicability to a wide range of salt species can benefit from the development of low-water-transport IEMs to minimize parasitic water transport, better understanding of crystallization kinetics and EDC behaviour with mixed-salt brines and realistic brines that contain fouling and scaling agents.

Methods

EDC experimental system description

A commercial ED cell (ED 64002, PCCell GmbH) was employed, with an effective membrane size of 8 × 8 cm and a spacer thickness of 0.45 mm. For the proof-of-concept experiments, the ED cell comprises two pairs of standard IEMs, which include two CEMs contacting the terminal electrodes (namely terminal CEMs), two standard AEMs and one standard CEM. To resist oxidative species and withstand a certain differential pressure, two terminal CEMs were placed near the electrode. The operating conditions were: current density at 20, 40 and 60 mA cm^{-2}, 2 litres of 63.5 g l^{-1} Na_2SO_4 diluate and 1 litre of saturated Na_2SO_4 brine.

For experiments of different salts in section 'Crystallizability criterion', five pairs of standard IEMs were configured initially to accelerate

the ion transport and changes of brine concentration, including two terminal CEMs, five standard AEMs and four standard CEMs. The operating conditions for each salt (Na_2SO_4, K_2SO_4, KNO_3, KCl and NaCl) were as follows: current density at 40 mA cm^{-2}, 4 litres of 0.6 M diluate and 1 litre of saturated brine. Then additional three experiments were performed for KCl and NaCl crystallization with five pairs of low-water-transfer IEMs and the operating conditions included: (1) current density at 40 mA cm^{-2}, 4 litres of 0.6 M KCl diluate and 1 litre of saturated KCl brine; (2) current density at 60 mA cm^{-2}, 4 litres of 1.2 M KCl diluate and 0.5 litres of saturated KCl brine and (3) current density at 80 mA cm^{-2}, 4 litres of 4 M NaCl diluate and 0.5 litres of saturated NaCl brine. The detailed setups of experiments are listed in Supplementary Table 9.

In the MF cell, an 11 × 6 cm stainless-steel mesh filter with pore size of 5 µm (316 Stainless Steel, McMaster) was used to filter the effluent of the crystallizer to avoid crystal clogging in the ED cell and/or redissolving in the ED cell with a slightly higher temperature due to resistive heat generation (Supplementary Section 4). A peristaltic pump (MFLX77200-62, MasterFlex) was used for circulating the brine streams with crystals at a speed of 1.2 l min^{-1}. The permeate through the mesh filter was pumped into the ED cell, while the retentate was pumped back into the crystallizer. The flow rate of solutions in the ED cell was 200 ml min^{-1}, and the stirring speed in the crystallizer was maintained at around 300 r.p.m. A Mettler-Toledo conductivity meter (Inlab 731 ISM) was used for measuring conductivity in the feed stream. A Lavolta BPS-305 DC power was applied in a constant current mode (1.28, 2.56 and 3.84 A for current densities of 20, 40 and 60 mA cm^{-2}, respectively). The brine stream was recirculated between the brine channel of the ED cell and the crystallizer (that is, a stainless-steel vessel to maximize heat transfer) placed in a water bath that was connected to a chiller for temperature control. In the continuous mode, the temperature of the brine stream was maintained at 18 °C, while in the batch mode, no temperature control was applied during the operation of experiments.

TSS sampling

The brine was sampled per hour in both continuous and batch modes. In the continuous mode, to minimize uneven distribution of crystals in the container, three samples (each 20 ml) from different positions (top, middle and bottom) of the crystallizer were collected by a syringe. The average TSS of three samples would be regarded as the TSS at the time of sampling. The samples were filtered through a stainless-steel mesh filter loaded in a stir cell (Amicon Stirred Cell 50 ml Seal Kit, Millipore Sigma). The crystals on the membrane were dried in an oven and then weighed until the weight did not change. The retentate solution was not sent back to the brine. In batch mode, samples were directly obtained from the brine stream and placed into an external water bath with a constant temperature at 18 °C. The conductivity of the samples was measured until it did not further decrease (that is, the crystals were precipitated completely). Then the samples were filtered through Whatman Grade 5 filter and then weighted after oven dry.

TSS quantification

To accelerate the production of salt crystals at 18 °C, we provided a supersaturated brine solution with its initial salt concentration corresponding to the salt solubility at 20 °C (Supplementary Table 1). Therefore, the TSS production can be ascribed to two reasons: (1) the increase of brine concentration during the ED process, and (2) salt solubility difference between 18 °C and 20 °C. To quantify the real TSS (TSS_R) due to concentration increase, the extra component, namely 'background TSS (TSS_B)', should be determined and then subtracted from the measured TSS values (TSS_M), as shown in the following equation:

$$TSS_R = TSS_M - TSS_B \tag{1}$$

For the continuous mode, TSS_B was tested in our EDC setup with no current density applied. To avoid the diffusion/osmosis between the brine and diluate/rinse streams, only the brine stream was pumped into the ED cell and circulated for 3 h at 18 °C. Samples were collected at 60, 120 and 180 min, and the measured TSS would be set as TSS_B.

For the batch mode, TSS_B was measured in normal EDC experiments described above. For each experiment, four samples were collected from the brine stream at 0, 60, 120 and 180 min, respectively. The collected samples were then cooled down to 18 °C in the water bath. The TSS value measured for the sample collected at 0 min was set as TSS_B. The detailed data and calculation processes are shown in Supplementary Section 2.

In TSS measurement, the balance (ME104E, Mettler Toledo) and syringe were used with a precision of 0.1 mg and 1 ml, respectively. The equation of TSS measurement is shown below:

$$TSS = \frac{m_{cry}}{V_{brine}} \tag{2}$$

where m_{cry} is the mass of crystals after oven-dry, V_{brine} is the volume of brine samples (20 ml).

As the coefficient of variation (COV) of m_{cry} is negligible compared with that of V_{brine} ($\frac{\sigma_m}{m_{cry}} \ll \frac{\sigma_V}{V_{brine}}$), the uncertainty value COV of TSS, $\frac{\sigma_{TSS}}{TSS}$, can be represented as equation (3):

$$\frac{\sigma_{TSS}}{TSS} = \sqrt{\left(\frac{\sigma_m}{m_{cry}}\right)^2 + \left(\frac{\sigma_V}{V_{brine}}\right)^2} \approx \frac{\sigma_V}{V_{brine}} \tag{3}$$

With V_{brine} of 20 ml and σ_V of 1 ml, the COV of TSS ($\frac{\sigma_{TSS}}{TSS}$) is 5%.

Energy consumption analysis of the EDC and EDC-RO systems

Energy consumption of the bench-scale EDC system accounts for the electric energy consumed in the ED cell and was calculated with experimental voltage drop over repeating units and TSS production data. Energy consumption on electrode reactions was excluded. The overall energy consumption of the EDC-RO treatment train at the steady-state operation was estimated as the sum of energy consumption for crystallization via EDC unit and concentration of the diluate effluent from the ED cell via RO unit. Crystal yield from bench-scale experiments was used to estimate process-scale TSS production. Pressure exchanger was considered to recover energy from the RO brine when estimating RO unit energy consumption. More modelling details can be found in Supplementary Sections 8 and 9.

Reporting summary

Further information on research design is available in the Nature Portfolio Reporting Summary linked to this article.

Data availability

Source data are provided with this paper.

Code availability

No code is used in the current study.

References

1. Tong, T. Z. & Elimelech, M. The global rise of zero liquid discharge for wastewater management: drivers, technologies, and future directions. *Environ. Sci. Technol.* **50**, 6846–6855 (2016).
2. Shah, K. M. et al. Drivers, challenges, and emerging technologies for desalination of high-salinity brines: a critical review. *Desalination* **538**, 115827 (2022).
3. Karanikola, V., Boo, C., Rolf, J. & Elimelech, M. Engineered slippery surface to mitigate gypsum scaling in membrane distillation for treatment of hypersaline industrial wastewaters. *Environ. Sci. Technol.* **52**, 14362–14370 (2018).

4. Tian, W. D., Wang, X., Fan, C. Y. & Cui, Z. Optimal treatment of hypersaline industrial wastewater via bipolar membrane electrodialysis. *ACS Sustain. Chem. Eng.* **7**, 12358–12368 (2019).
5. Chang, H. Q. et al. Potential and implemented membrane-based technologies for the treatment and reuse of flowback and produced water from shale gas and oil plays: a review. *Desalination* **455**, 34–57 (2019).
6. Tong, T. Z., Carlson, K. H., Robbins, C. A., Zhang, Z. Y. & Du, X. W. Membrane-based treatment of shale oil and gas wastewater: the current state of knowledge. *Front. Environ. Sci. Eng.* **13**, 63 (2019).
7. Shemer, H. & Semiat, R. Sustainable RO desalination—energy demand and environmental impact. *Desalination* **424**, 10–16 (2017).
8. Ellsworth, W. L. Injection-induced earthquakes. *Science* **341**, 1225942 (2013).
9. Scanlon, B. R., Weingarten, M. B., Murray, K. E. & Reedy, R. C. Managing basin-scale fluid budgets to reduce injection-induced seismicity from the recent U.S. shale oil revolution. *Seismol. Res. Lett.* **90**, 171–182 (2018).
10. Davenport, D. M., Deshmukh, A., Werber, J. R. & Elimelech, M. High-pressure reverse osmosis for energy-efficient hypersaline brine desalination: current status, design considerations, and research needs. *Environ. Sci. Technol. Lett.* **5**, 467–475 (2018).
11. Mauter, M. S. & Fiske, P. S. Desalination for a circular water economy. *Energy Environ. Sci.* **13**, 3180–3184 (2020).
12. Wang, R. & Lin, S. Thermodynamics and energy efficiency of zero liquid discharge. *ACS ES&T Eng.* **2**, 1491–1503 (2022).
13. Mickley, M. *Survey of High-Recovery and Zero Liquid Discharge Technologies for Water Utilities* (WateReuse, 2008).
14. Burbano, A. & Brankhuber, P. *Demonstration of Membrane Zero Liquid Discharge for Drinking Water Systems—A Literature Review* (The Water Research Foundation, 2014).
15. McGinnis, R. L., Hancock, N. T., Nowosielski-Slepowron, M. S. & McGurgan, G. D. Pilot demonstration of the NH_3/CO_2 forward osmosis desalination process on high salinity brines. *Desalination* **312**, 67–74 (2013).
16. What is zero liquid discharge & why is it important? *Saltworks* https://www.saltworkstech.com/articles/what-is-zero-liquid-discharge-why-is-it-important/ (2018).
17. Xu, T. & Huang, C. Electrodialysis-based separation technologies: a critical review. *AlChE J.* **54**, 3147–3159 (2008).
18. Strathmann, H. Electrodialysis, a mature technology with a multitude of new applications. *Desalination* **264**, 268–288 (2010).
19. Zhang, X. et al. Near-zero liquid discharge of desulfurization wastewater by electrodialysis-reverse osmosis hybrid system. *J. Water Process. Eng.* **40**, 101962 (2021).
20. Reig, M. et al. Concentration of NaCl from seawater reverse osmosis brines for the chlor-alkali industry by electrodialysis. *Desalination* **342**, 107–117 (2014).
21. Jiang, C., Wang, Y., Zhang, Z. & Xu, T. Electrodialysis of concentrated brine from RO plant to produce coarse salt and freshwater. *J. Membr. Sci.* **450**, 323–330 (2014).
22. Lin, S. Energy efficiency of desalination: fundamental insights from intuitive interpretation. *Environ. Sci. Technol.* **54**, 76–84 (2019).
23. Tong, T., Wallace, A. F., Zhao, S. & Wang, Z. Mineral scaling in membrane desalination: mechanisms, mitigation strategies, and feasibility of scaling-resistant membranes. *J. Membr. Sci.* **579**, 52–69 (2019).
24. Rolf, J. et al. Inorganic scaling in membrane desalination: models, mechanisms, and characterization methods. *Environ. Sci. Technol.* **56**, 7484–7511 (2022).
25. Tedesco, M., Hamelers, H. V. M. & Biesheuvel, P. M. Nernst–Planck transport theory for (reverse) electrodialysis: II. Effect of water transport through ion-exchange membranes. *J. Membr. Sci.* **531**, 172–182 (2017).
26. Jiang, C., Wang, Q., Li, Y., Wang, Y. & Xu, T. Water electro-transport with hydrated cations in electrodialysis. *Desalination* **365**, 204–212 (2015).
27. Porada, S., van Egmond, W. J., Post, J. W., Saakes, M. & Hamelers, H. V. M. Tailoring ion exchange membranes to enable low osmotic water transport and energy efficient electrodialysis. *J. Membr. Sci.* **552**, 22–30 (2018).
28. Epsztein, R., Shaulsky, E., Qin, M. & Elimelech, M. Activation behavior for ion permeation in ion-exchange membranes: role of ion dehydration in selective transport. *J. Membr. Sci.* **580**, 316–326 (2019).
29. Sun, B., Zhang, M., Huang, S., Wang, J. & Zhang, X. Limiting concentration during batch electrodialysis process for concentrating high salinity solutions: A theoretical and experimental study. *Desalination* **498**, 114793 (2021).
30. Kingsbury, R. et al. Influence of water uptake, charge, manning parameter, and contact angle on water and salt transport in commercial ion exchange membranes. *Ind. Eng. Chem. Res.* **58**, 18663–18674 (2019).
31. Jones, A. G. *Crystallization Process Systems* (Elsevier, 2002).

Acknowledgements

This material is based on the work supported by the National Alliance for Water Innovation (NAWI), funded by the US Department of Energy, Office of Energy Efficiency and Renewable Energy (EERE), Advanced Manufacturing Office, under Funding Opportunity Announcement Number DE-FOA-0001905. The views expressed herein do not necessarily represent the views of the US Department of Energy or the US Government.

Author contributions

S.L. and T.T. conceived the idea and designed the research. X.Z., Y. Yao. and T.H. carried out the experiment. R.W. performed the energy consumption analysis. All authors participated in the discussion and writing of the paper.

Competing interests

We are in the process of filing a provisional patent application based on this work.

Additional information

Supplementary information The online version contains supplementary material available at https://doi.org/10.1038/s44221-023-00095-4.

Correspondence and requests for materials should be addressed to Tiezheng Tong or Shihong Lin.

Peer review information *Nature Water* thanks Mohammed Elhashimi, How Yong Ng and Natasha Wright for their contribution to the peer review of this work.

nature portfolio

Corresponding author(s): Dr. Shihong Lin, Dr. Tiezheng Tong

Last updated by author(s): May 8, 2023

Reporting Summary

Nature Portfolio wishes to improve the reproducibility of the work that we publish. This form provides structure for consistency and transparency in reporting. For further information on Nature Portfolio policies, see our Editorial Policies and the Editorial Policy Checklist.

Statistics

For all statistical analyses, confirm that the following items are present in the figure legend, table legend, main text, or Methods section.

n/a	Confirmed	
☐	☒	The exact sample size (*n*) for each experimental group/condition, given as a discrete number and unit of measurement
☒	☐	A statement on whether measurements were taken from distinct samples or whether the same sample was measured repeatedly
☒	☐	The statistical test(s) used AND whether they are one- or two-sided *Only common tests should be described solely by name; describe more complex techniques in the Methods section.*
☒	☐	A description of all covariates tested
☒	☐	A description of any assumptions or corrections, such as tests of normality and adjustment for multiple comparisons
☐	☒	A full description of the statistical parameters including central tendency (e.g. means) or other basic estimates (e.g. regression coefficient) AND variation (e.g. standard deviation) or associated estimates of uncertainty (e.g. confidence intervals)
☒	☐	For null hypothesis testing, the test statistic (e.g. *F*, *t*, *r*) with confidence intervals, effect sizes, degrees of freedom and *P* value noted *Give P values as exact values whenever suitable.*
☒	☐	For Bayesian analysis, information on the choice of priors and Markov chain Monte Carlo settings
☒	☐	For hierarchical and complex designs, identification of the appropriate level for tests and full reporting of outcomes
☒	☐	Estimates of effect sizes (e.g. Cohen's *d*, Pearson's *r*), indicating how they were calculated

Our web collection on statistics for biologists contains articles on many of the points above.

Software and code

Policy information about availability of computer code

Data collection	No software was used.
Data analysis	The software PHREEQC Interactive 3.7.3-15968 was used to calculate the saturation index of gypsum.

For manuscripts utilizing custom algorithms or software that are central to the research but not yet described in published literature, software must be made available to editors and reviewers. We strongly encourage code deposition in a community repository (e.g. GitHub). See the Nature Portfolio guidelines for submitting code & software for further information.

Data

Policy information about availability of data

All manuscripts must include a data availability statement. This statement should provide the following information, where applicable:

- Accession codes, unique identifiers, or web links for publicly available datasets
- A description of any restrictions on data availability
- For clinical datasets or third party data, please ensure that the statement adheres to our policy

Source data for all figure(s) are provided with the paper.

Human research participants

Policy information about studies involving human research participants and Sex and Gender in Research.

Reporting on sex and gender	The study doesn't involve human research participants.
Population characteristics	The study doesn't involve human research participants.
Recruitment	The study doesn't involve human research participants.
Ethics oversight	The study doesn't involve human research participants.

Note that full information on the approval of the study protocol must also be provided in the manuscript.

Field-specific reporting

Please select the one below that is the best fit for your research. If you are not sure, read the appropriate sections before making your selection.

☐ Life sciences ☐ Behavioural & social sciences ☒ Ecological, evolutionary & environmental sciences

For a reference copy of the document with all sections, see nature.com/documents/nr-reporting-summary-flat.pdf

Ecological, evolutionary & environmental sciences study design

All studies must disclose on these points even when the disclosure is negative.

Study description	*Briefly describe the study. For quantitative data include treatment factors and interactions, design structure (e.g. factorial, nested, hierarchical), nature and number of experimental units and replicates.*
Research sample	*Describe the research sample (e.g. a group of tagged Passer domesticus, all Stenocereus thurberi within Organ Pipe Cactus National Monument), and provide a rationale for the sample choice. When relevant, describe the organism taxa, source, sex, age range and any manipulations. State what population the sample is meant to represent when applicable. For studies involving existing datasets, describe the data and its source.*
Sampling strategy	*Note the sampling procedure. Describe the statistical methods that were used to predetermine sample size OR if no sample-size calculation was performed, describe how sample sizes were chosen and provide a rationale for why these sample sizes are sufficient.*
Data collection	*Describe the data collection procedure, including who recorded the data and how.*
Timing and spatial scale	*Indicate the start and stop dates of data collection, noting the frequency and periodicity of sampling and providing a rationale for these choices. If there is a gap between collection periods, state the dates for each sample cohort. Specify the spatial scale from which the data are taken*
Data exclusions	*If no data were excluded from the analyses, state so OR if data were excluded, describe the exclusions and the rationale behind them, indicating whether exclusion criteria were pre-established.*
Reproducibility	*Describe the measures taken to verify the reproducibility of experimental findings. For each experiment, note whether any attempts to repeat the experiment failed OR state that all attempts to repeat the experiment were successful.*
Randomization	*Describe how samples/organisms/participants were allocated into groups. If allocation was not random, describe how covariates were controlled. If this is not relevant to your study, explain why.*
Blinding	*Describe the extent of blinding used during data acquisition and analysis. If blinding was not possible, describe why OR explain why blinding was not relevant to your study.*

Did the study involve field work? ☐ Yes ☒ No

Reporting for specific materials, systems and methods

We require information from authors about some types of materials, experimental systems and methods used in many studies. Here, indicate whether each material, system or method listed is relevant to your study. If you are not sure if a list item applies to your research, read the appropriate section before selecting a response.

Materials & experimental systems

n/a	Involved in the study
☒	☐ Antibodies
☒	☐ Eukaryotic cell lines
☒	☐ Palaeontology and archaeology
☒	☐ Animals and other organisms
☒	☐ Clinical data
☒	☐ Dual use research of concern

Methods

n/a	Involved in the study
☒	☐ ChIP-seq
☒	☐ Flow cytometry
☒	☐ MRI-based neuroimaging